Hyperspectral Denoising: From Conventional Techniques Towards Deep Learning Ones

Behnood Rasti[1], Pedram Ghamisi[1,2]

[1]Helmholtz-Zentrum Dresden-Rossendorf, Helmholtz Institute Freiberg for Resource Technology, Machine Learning Group, Chemnitzer Straße 40, 09599 Freiberg, Germany),

[2]Institute of Advanced Research in Artificial Intelligence (IARAI), Landstraßer Hauptstraße 5, 1030 Vienna, Austria

Abstract

In this paper, we provide an overview on hyperspectral image denoising techniques. Additionally, we compare the conventional techniques with the deep learning ones applied to simulated and real datasets. The comparisons are performed in terms of signal to noise ratio and spectral angle distance for a simulated noisy dataset. Finally, we demonstrate the visual performance of the techniques applied to a real hyperspectral dataset. The results show that the established low-rank conventional techniques outperform the recent deep learning-based techniques used in the experiments.

Keywords

Hyperspectral Denoising, Deep Learning, Self-supervised Learning,

1. Introduction

In the past decade, hyperspectral image (HSI) denoising has considerably evolved, from 2D and 3D full-rank conventional methods to low-rank ones. Recent advances in deep learning-based techniques have considerably influenced the application of denoising in the computer vision community. However, HSIs have unique characteristics which distinguish them from the other digital images, e.g., RGB images. In this article, we provide an overview of the HSI denoising techniques. Additionally, we compare the conventional denoising techniques with the deep-learning ones.

2. Hyperspectral Denoising

An HSI can be modeled using

$$\mathbf{H} = \mathbf{X} + \mathbf{N}, \tag{1}$$

where $\mathbf{H} \in \mathbb{R}^{n \times p}$ contains the observed spectral bands in its columns, $\mathbf{X} \in \mathbb{R}^{n \times p}$ is the noise free signal which needs to be estimated, and $\mathbf{N} \in \mathbb{R}^{n \times p}$ denotes the noise. The denoising task is to estimate the unknown noise-free signal $\mathbf{X}$.

Generally, hyperspectral denoising is an inverse image restoration task, which can be formulated as

$$\hat{\mathbf{X}} = \arg\min_{\mathbf{X}} \frac{1}{2} \|\mathbf{H} - \mathbf{X}\|_F^2 + \lambda \phi(\mathbf{X}), \tag{2}$$

where λ determines the trade-off between the fidelity term and the penalty term $\phi(\mathbf{X})$. We assume that the noise is uncorrelated spectrally, i.e., $\mathbf{\Omega} = \text{diag}\left(\sigma_1^2, \sigma_2^2, \ldots, \sigma_p^2\right)$ is the noise covariance matrix where σ_i is the noise standard deviation of band i.

2.1. Conventional Techniques

The conventional denoising approaches can be divided into two independent groups: full-rank and low-rank approaches.

2.1.1. Full-rank Approaches

Full-rank denoising approaches assume that $\mathbf{X}$ is full-rank. Since HSI is a collection of spectral bands, denoising approaches that have been developed for gray scale images (e.g., wavelet denoising and mean/median filtering) can be applied on HSIs band by band. However, rich spectral information existing in HSIs is ignored in this way. On the other hand, HSI is also a combination of spectral pixels and, therefore, 1D signal denoising approaches such as multiple linear regression (MLR) proposed in [1] can be applied on spectral pixel vectors and, therefore, spatial information is ignored in this way. As a result, HSI denoising considerably benefits by exploiting both spatial and spectral information. 3D modeling and filtering such as 3D wavelets [2] and 3D (blockwise) nonlocal sparse denoising (Nonlocal SR) methods [3] are the earliest attempts for spatial-spectral denoising approaches. Later on, penalized least squares exploiting spatial [4],

CDCEO 2021: 1st Workshop on Complex Data Challenges in Earth Observation, November 1, 2021, Virtual Event, QLD, Australia.

b.rasti@hzdr.de (B. Rasti); pedram.ghamisi@iarai.ac.at (P. Ghamisi)

https://www.researchgate.net/profile/Behnood-Rasti (B. Rasti); http://www.pedram-ghamisi.com/ (P. Ghamisi)

0000-0002-1091-9841 (B. Rasti); 0000-0003-1203-741X (P. Ghamisi)

spectral [5], and spatial-spectral penalties [6] were proposed for HSI denoising. An efficient edge-preserving denoising approach is obtained with a prior $\phi(\mathbf{X})$ in (2) corresponding to the total variation (TV) of the signal [7].

Several TV denoising approaches including Cubic TV (CTV) [8, 9] and spatio-spectral TV [10] were adapted for HSI denoising to capture the spectral correlation using TV.

2.1.2. Low-Rank Approaches

Low-rank models assume that $\mathbf{X}$ is low-rank so to capture the high spectral correlation of HSI. The low-rank property can be applied in two different ways:

(1) Using a low-rank model

$$\mathbf{H} = \mathbf{F}\mathbf{V}^T + \mathbf{N}, \tag{3}$$

where $\mathbf{F}$ and $\mathbf{V}$ are of rank r ($r \ll \min\{n, p\}$).

(2) Using a low-rank penalty or constraint such as the nuclear norm in the cost function:

$$\hat{\mathbf{X}} = \arg\min_{\mathbf{X}} \ \frac{1}{2}\|\mathbf{H} - \mathbf{X}\|_F^2 + \lambda_1\phi(\mathbf{X}) + \lambda_2\|\mathbf{X}\|_*, \tag{4}$$

where $\|\mathbf{X}\|_*$ is the nuclear-norm of the matrix $\mathbf{X}$, obtained by the sum of the singular values.

Several hyperspectral denoising approaches were proposed using Tucker3 decomposition [11, 12]. In [13], a wavelet-based low-rank model and ℓ_1 regularization was proposed for HSI denoising (SVDSRR). An automatic hyperspectral restoration technique (HyRes) was proposed in [14] using the ℓ_1 penalized least squares and a low-rank wavelet-based model.

In [15], the wavelet-based reduced-rank (WSRRR) model was proposed for simultaneous HSI denoising and feature extraction using a non-convex optimization problem.

Low-rank TV regularization was also proposed in [16, 17] for both HSI denoising and feature extraction.

Noise-adjusted image recovery using low-rank matrix approximation (NAIRLMA) was suggested in [18] exploiting both low-rank and sparsity norms. Fast hyperspectral denoising (FastHyDe) proposed in [19] is also a low-rank technique that first project the HSI into a subspace and, then, applies BM3D denoising [20] on the eigen images. Spectral linear unmixing techniques are also considered as a low-rank HSI denoiser [21, 22].

2.2. Deep learning-based Techniques

Deep learning-based denoising approaches are the state-of-the-art in the signal and image processing community but they have been mostly developed for RGB images. Although they can usually be used for HSI denoising, they cannot model the specific characteristics of HSIs, e.g., low-rank and spectral dependency.

Since 2017, deep learning have been utilized for HSI denoising. The fundamental challenge for applying deep learning for HSI denoising is the high-dimensionality of HSIs. The high-dimensionality leads to a huge number of trainable parameters but, at the same time, the number of training samples is often limited in the remote sensing community. The imbalance between the number of training samples and trainable parameters makes the network training cumbersome to achieve a universal DL-based denoising technique for HSIs [23]. With regard to the availability of training samples, HSI deep-learning-based denoising techniques can be split into two categories:

2.2.1. Unsupervised/self-supervised

The unsupervised techniques do not utilize any training set and only rely on the observed image. One example of such approaches is deep HSI prior (HSI-DIP) introduced in [24]. HSI-DIP is based on *deep image prior* (DIP) [25], which utilizes a convolutional encoder-decoder network to implicitly induce a universal regularizer (the so-called image prior) in inverse problems including denoising. In [24], 2D convolution was extended to a 3D one to model the specific characteristics of HSIs, however, it was not as efficient as the 2D version. Self-supervised techniques are dependent on the observed image for training while they create their own training sets from the observed noisy image. In [26], a self-supervised (Zero-shot) denoising technique was introduced for HSIs.

2.2.2. Supervised

These techniques demand training sets to train the network. Most of the deep-learning-based denoising techniques are supervised and their performances are highly dependent on the availability of a high number of training data. In HSI denoising, the deep networks are trained in three ways: (1) using a database by collecting many patches [27], (2) using a database containing many real HSIs such as ICVL [28] developed in [29], or (3) using a database by simulating HSIs based on RGB images using deep generative networks [30]. A spatial–spectral deep residual CNN (HSID-CNN) was introduced in [27] in which 2D and 3D convolutional filters were utilized to model spatial and spatial-spectral correlation in HSIs.

A 3D U-Net was introduced in [30] based on 2D convolutional filtering in spatial direction and 1D convolutional filtering in the spectral direction. A single model denoising CNN-based framework (SDeCNN) was introduced in [31]. In SDeCNN, spectral channels were extended along the spectral direction in the first place so that all spectral channels have centered by the same number of adjacent bands. Then, one band at a time was restored by applying the CNN on a downsampled HSI.

2.3. Experimental Results

Here, we compare the results of different hyperspectral denoising algorithms including 3D Wavelet [2], FORPDN [5], SSTV [10], NAIRLMA [18], HyRes [14], HSI-DIP [24], FastHyDe [19], and SDeCNN [31]. 3D wavelets, FORPDN, and HyRes are parameter-free techniques. We set the subspace dimension to 10 for FastHyDe. For HSI-DIP, all the hyperparameters and the layers of the encoder-decoder architecture are adjusted as suggested in [25] to optimize the performance. In the case of SDeCNN, we set the noise parameter σ to 1 since it gives the best results for the simulated data while, for the real dataset, we used the default value suggested by its authors i.e., $\sigma = 20$.

The hyperspectral denoising techniques are applied on a simulated noisy dataset and the results are compared based on different levels of the noise power, i.e., PSNR=20, 30, and 40 dB. The uncorrelated (the same variance for all bands) zero-mean Gaussian noise was added to a portion of the Washington DC Mall dataset. Fig. 1 (a) and (b) compare the results of the techniques in terms of PSNR and spectral angle distance (SAD). The results are mean values over five experiments. The standard deviations are shown using error bars. The results confirm that the low-rank techniques used in the experiments outperform the other techniques in terms of both PSNR and SAD. Additionally, HSI-DIP outperforms the full-rank conventional techniques, i.e., 3D wavelet, FORPDN, and SSTV. On the other hand, SDeCNN performs poorly.

For the real HSI denoising experiment, we apply all the denoising techniques on the Indian Pines dataset. The results of denoising for band 1 are compared visually in Fig. 2. The outcome of the visual comparison can be summarized as follows: NAIRLMA fails to restore band 1. 3D Wavelet restores band 1 with moderate visual quality. SDeCNN shows the poorest results. Band 1 is highly over-smoothed. We should note that SDeCNN was also applied to Indian Pines in [31], however, the authors removed the noisy bands from the dataset (resulting in a dataset having 206 bands) before applying the denoising techniques. Here, all 220 bands were used to evaluate the methods since the aim of HSI denoising techniques is to recover all the corrupted bands. SSTV, HyRes, and FastHyDe successfully and similarly reconstruct band 1. HSI-DIP also restores band 1 successfully, however, the restored band seems over-smoothed and blurred. FORPDN outperforms the other techniques visually. We should note that considering numerous bands existing in HSIs, this comparison might not reflect the performance of the techniques on the whole image. Band 1 is selected for comparison since it is noisy and it is often more challenging to recover the first and last few bands in HSIs due to the absence of the adjacent bands.

2.3.1. Discussion and Conclusion

The superiority of the low-rank techniques compared to the full-rank ones can be attributed to the spectral redundancy of HSIs. Low-rank techniques capture the most variations of the signal by projecting it into a subspace which helps to decorrelate the signal spectrally from the noise. Denoising techniques such as HyRes and FastHyDe further denoise the signal spatially in its subspace. HSI-DIP is an unsupervised denoising technique, i.e., the network is trained using the observed data. SDeCNN exploits only one CNN model which is trained based on one dataset. Therefore, SDeCNN cannot perform well for all types of HSI data with different noise levels. We should note that, in the case of HSIs in particular HSI denoising, the training is often challenging due to the absence or the limited number of training sets. Therefore, Low-rank-based HSI denoising techniques still outperform the deep learning-based ones.

3. Acknowledgments

The work of Behnood Rasti was funded by the Alexander-von-Humboldt-Stiftung/foundation.

References

[1] J. Bioucas-Dias, J. Nascimento, Hyperspectral subspace identification, IEEE Trans. Geos. Remote Sens 46 (2008) 2435 –2445.

[2] B. Rasti, J. R. Sveinsson, M. O. Ulfarsson, J. A. Benediktsson, Hyperspectral image denoising using 3D wavelets, in: IEEE IGARSS, 2012, pp. 1349–1352.

[3] Y. Qian, M. Ye, Hyperspectral imagery restoration using nonlocal spectral-spatial structured sparse representation with noise estimation, IEEE Jour. Sel. Top. App. Earth Obs. Remote Sens. 6 (2013) 499–515.

[4] A. Zelinski, V. Goyal, Denoising hyperspectral imagery and recovering junk bands using wavelets and sparse approximation, in: IEEE IGARSS, 2006, pp. 387 –390.

[5] B. Rasti, J. R. Sveinsson, M. O. Ulfarsson, J. A. Benediktsson, Hyperspectral image denoising using first order spectral roughness penalty in wavelet domain, IEEE Jour. Sel. Top. App. Earth Obs. Remote Sens. 7 (2014) 2458–2467.

[6] B. Rasti, J. R. Sveinsson, M. O. Ulfarsson, J. A. Benediktsson, Wavelet based hyperspectral image restoration using spatial and spectral penalties, in: Proc. SPIE, volume 8892, 2013, pp. 88920I–88920I–8.

[7] L. I. Rudin, S. Osher, E. Fatemi, Nonlinear total

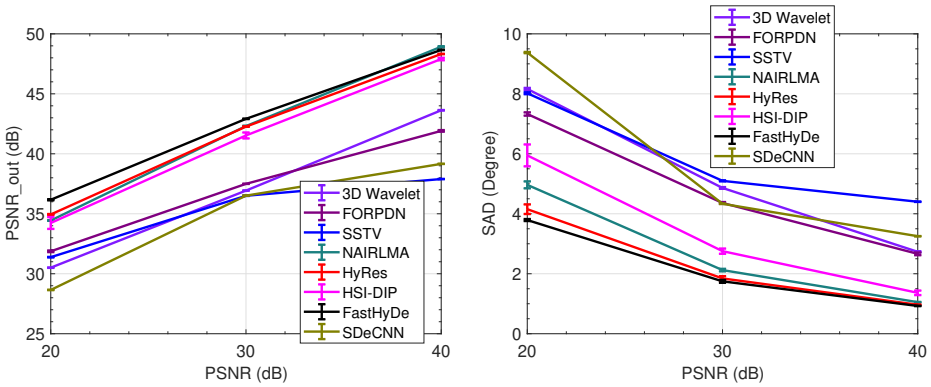

(a) PSNR (b) SAD

Figure 1: Results of denoising on the simulated Washington DC Mall image for three different input noise levels (i.e., PSNR=20, 30, and 40 dB): (a) PSNR in dB (b) SAD in degree.

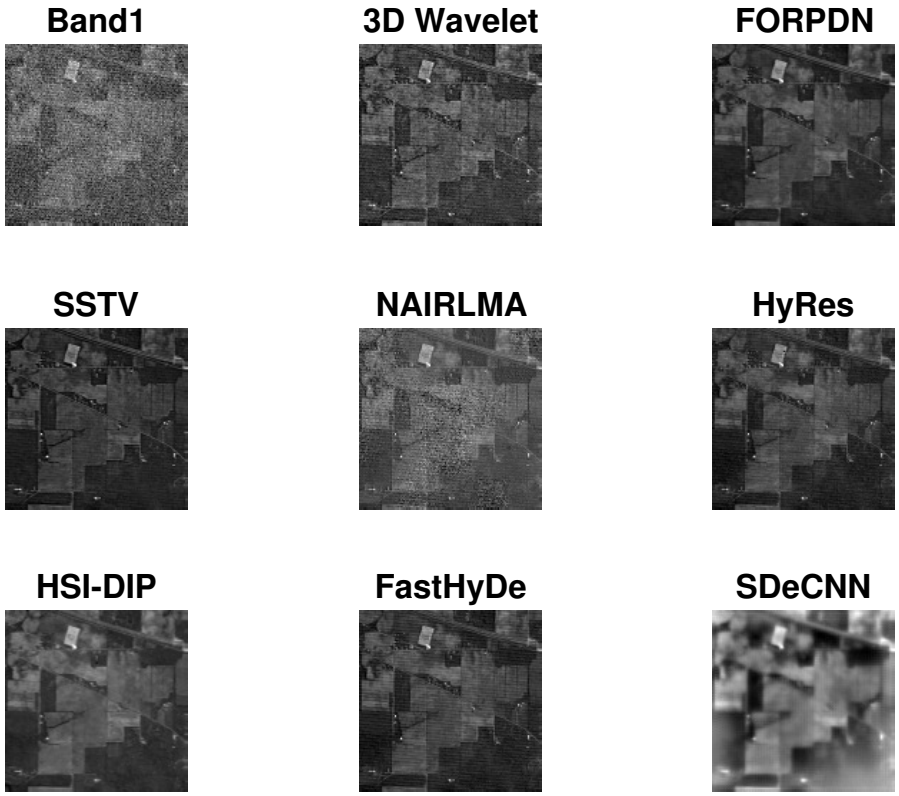

Figure 2: Results of denoising on Indian Pines. The first restored bands using different denoising techniques are visually compared with the observed noisy one.

variation based noise removal algorithms, Phys. D 60 (1992) 259–268.

[8] Q. Yuan, L. Zhang, H. Shen, Hyperspectral image denoising employing a spectral-spatial adaptive total variation model., IEEE Trans. Geos. Remote Sens 50 (2012) 3660–3677.

[9] H. Zhang, Hyperspectral image denoising with cubic total variation model, in: ISPRS Annals of

Photo., Remote Sens. Spatial Inf. Sci., volume I-7, 2012, pp. 95–98.

[10] H. K. Aggarwal, A. Majumdar, Hyperspectral image denoising using spatio-spectral total variation, IEEE Geos. Remote Sens. Lett. 13 (2016) 442–446. doi:10.1109/LGRS.2016.2518218.

[11] A. Karami, M. Yazdi, A. Zolghadre Asli, Noise reduction of hyperspectral images using kernel non-negative tucker decomposition, IEEE Jour. Sel. Top. Sig. Proc. 5 (2011) 487 –493.

[12] X. Liu, S. Bourennane, C. Fossati, Denoising of hyperspectral images using the parafac model and statistical performance analysis, IEEE Trans. Geos. Remote Sens 50 (2012) 3717–3724. doi:10.1109/TGRS.2012.2187063.

[13] B. Rasti, J. R. Sveinsson, M. O. Ulfarsson, J. A. Benediktsson, A new linear model and sparse regularization, in: IEEE IGARSS, 2013, pp. 457–460.

[14] B. Rasti, M. O. Ulfarsson, P. Ghamisi, Automatic hyperspectral image restoration using sparse and low-rank modeling, IEEE Geos. Remote Sens. Lett. PP (2017) 1–5. doi:10.1109/LGRS.2017.2764059.

[15] B. Rasti, J. Sveinsson, M. Ulfarsson, Wavelet-based sparse reduced-rank regression for hyperspectral image restoration, IEEE Trans. Geos. Remote Sens 52 (2014) 6688–6698.

[16] B. Rasti, J. R. Sveinsson, M. O. Ulfarsson, Total variation based hyperspectral feature extraction, in: IEEE IGARSS, 2014, pp. 4644–4647.

[17] B. Rasti, Sparse Hyperspectral Image Modeling and Restoration, Ph.D. thesis, Dep. of Electrical and Computer Engineering, University of Iceland, 2014.

[18] W. He, H. Zhang, L. Zhang, H. Shen, Hyperspectral image denoising via noise-adjusted iterative low-rank matrix approximation, IEEE Jour. Sel. Top. App. Earth Obs. Remote Sens. 8 (2015) 3050–3061. doi:10.1109/JSTARS.2015.2398433.

[19] L. Zhuang, J. M. Bioucas-Dias, Fast hyperspectral image denoising and inpainting based on low-rank and sparse representations, IEEE Jour. Sel. Top. App. Earth Obs. Remote Sens. 11 (2018) 730–742. doi:10.1109/JSTARS.2018.2796570.

[20] K. Dabov, A. Foi, V. Katkovnik, K. Egiazarian, Image Denoising by Sparse 3-D Transform-Domain Collaborative Filtering, IEEE Trans. Imag. Proc. 16 (Agu.) 2080–2095.

[21] B. Rasti, B. Koirala, P. Scheunders, P. Ghamisi, How hyperspectral image unmixing and denoising can boost each other, Remote Sens. 12 (2020) 1728. URL: http://dx.doi.org/10.3390/rs12111728. doi:10.3390/rs12111728.

[22] D. Cerra, R. Müller, P. Reinartz, Noise reduction in hyperspectral images through spectral unmixing, IEEE Geos. Remote Sens. Lett. 11 (2014) 109–113.

[23] B. Rasti, Y. Chang, E. Dalsasso, L. Denis, P. Ghamisi, Image restoration for remote sensing: Overview and toolbox (2021). arXiv:2107.00557.

[24] O. Sidorov, J. Y. Hardeberg, Deep hyperspectral prior: Single-image denoising, inpainting, super-resolution, in: IEEE/CVF International Conference on Computer Vision Workshop (ICCVW), 2019, pp. 3844–3851. doi:10.1109/ICCVW.2019.00477.

[25] D. Ulyanov, A. Vedaldi, V. Lempitsky, Deep image prior, International Journal of Computer Vision 128 (2020) 1867–1888. URL: http://dx.doi.org/10.1007/s11263-020-01303-4. doi:10.1007/s11263-020-01303-4.

[26] R. Imamura, T. Itasaka, M. Okuda, Zero-shot hyperspectral image denoising with separable image prior, in: 2019 IEEE/CVF International Conference on Computer Vision Workshop (ICCVW), 2019, pp. 1416–1420. doi:10.1109/ICCVW.2019.00178.

[27] Q. Yuan, Q. Zhang, J. Li, H. Shen, L. Zhang, Hyperspectral image denoising employing a spatial–spectral deep residual convolutional neural network, IEEE Trans. Geos. Remote Sens. 57 (2019) 1205–1218. doi:10.1109/TGRS.2018.2865197.

[28] B. Arad, O. Ben-Shahar, Sparse recovery of hyperspectral signal from natural rgb images, in: European Conference on Computer Vision, Springer, 2016, pp. 19–34.

[29] Y. Chang, L. Yan, H. Fang, S. Zhong, W. Liao, Hsidenet: Hyperspectral image restoration via convolutional neural network, IEEE Trans. Geos. Remote Sens. 57 (2019) 667–682. doi:10.1109/TGRS.2018.2859203.

[30] W. Dong, H. Wang, F. Wu, G. Shi, X. Li, Deep spatial–spectral representation learning for hyperspectral image denoising, IEEE Trans. Comput. Imaging 5 (2019) 635–648. doi:10.1109/TCI.2019.2911881.

[31] A. Maffei, J. M. Haut, M. E. Paoletti, J. Plaza, L. Bruzzone, A. Plaza, A single model cnn for hyperspectral image denoising, IEEE Trans. Geos. Remote Sens. 58 (2020) 2516–2529. doi:10.1109/TGRS.2019.2952062.

A. Online Resources

The sources for the denoising toolbox to reproduce the results are available via

- https://github.com/BehnoodRasti/Hyperspectral-Image-Denoising-Toolbox-V2.